

#### **OPEN ACCESS**

EDITED BY

Karen Elizabeth Nava-Castro, National Autonomous University of Mexico, Mexico

REVIEWED BY

Mariana Segovia-Mendoza, National Autonomous University of Mexico, Mexico Alexey Surov, Ruhr University Bochum, Germany

\*CORRESPONDENCE

Yuegin Chen

<sup>†</sup>These authors have contributed equally to

RECEIVED 24 June 2025
ACCEPTED 30 September 2025
PUBLISHED 20 October 2025

#### CITATION

Wang Z, Zhao F, Zhu L, Mao N, Wang W, Zhao W, Yu H, Li Y, Li C, Yue X, Chen Y and Sun Z (2025) A multifunctional MRI model based on IVIM and DKI predicts HIF-1 $\alpha$ , Ki-67, and VEGF status in breast carcinoma. *Front. Oncol.* 15:1652932. doi: 10.3389/fonc.2025.1652932

#### COPYRIGHT

© 2025 Wang, Zhao, Zhu, Mao, Wang, Zhao, Yu, Li, Li, Yue, Chen and Sun. This is an openaccess article distributed under the terms of the Creative Commons Attribution License (CC BY). The use, distribution or reproduction in other forums is permitted, provided the original author(s) and the copyright owner(s) are credited and that the original publication in this journal is cited, in accordance with accepted academic practice. No use, distribution or reproduction is permitted which does not comply with these terms.

# A multifunctional MRI model based on IVIM and DKI predicts HIF- $1\alpha$ , Ki-67, and VEGF status in breast carcinoma

Zhengtong Wang<sup>1†</sup>, Fan Zhao<sup>2†</sup>, Laimin Zhu<sup>1</sup>, Ning Mao<sup>3</sup>, Weiwei Wang<sup>1</sup>, Wenwen Zhao<sup>4</sup>, Hao Yu<sup>1</sup>, Yunxi Li<sup>1</sup>, Chongchong Li<sup>1</sup>, Xiuzheng Yue<sup>5</sup>, Yueqin Chen<sup>1\*</sup> and Zhanguo Sun<sup>1\*</sup>

<sup>1</sup>Department of Medical Imaging, Affiliated Hospital of Jining Medical University, Jining, China,

**Purpose:** The research aims to explore the predictive significance of diffusion-weighted imaging (DWI), diffusion kurtosis imaging (DKI), intravoxel incoherent motion (IVIM), and their integrated models in relation to Hypoxia-inducible factor-1 alpha (HIF- $1\alpha$ ), Ki-67, and vascular endothelial growth factor (VEGF) expression levels in breast carcinoma.

Materials and Methods: This retrospective study included 104 patients with pathologically confirmed breast carcinoma from our institution as the training set, while an external validation cohort of 91 eligible patients was recruited from another tertiary medical center. Two independently working radiologists analyzed IVIM-derived parameters apparent diffusion coefficient (ADC), true diffusion coefficient (D), perfusion-related diffusion coefficient (D\*), and perfusion fraction (f), and DKI-derived parameters mean diffusivity (MD) and mean kurtosis (MK). Receiver operating characteristic (ROC) curves were constructed for evaluation of diagnostic efficacy. The outcomes of the multivariate logistic regression model were employed to create a nomogram of the combined model for molecular marker status prediction.

**Results:** High expression levels of HIF-1 $\alpha$ , VEGF, and Ki-67 were consistently associated with lower D, MD, and ADC values, and higher perfusion-related D\*, f, and MK values (all P<0.05). ROC curve analysis showed that among the individual parameters, the D value exhibited the highest predictive efficacy (Area Under the Curve, AUC = 0.724). A D value  $\leq 0.88 \times 10^{-3}$  mm²/s should strongly suggest high HIF-1 $\alpha$  expression. ROC curve analysis revealed that the f parameter was the most powerful single indicator for predicting VEGF expression (AUC = 0.882). In clinical practice, an f value  $\geq 29.82\%$  can serve as a key imaging biomarker suggesting high VEGF expression, i.e., active tumor angiogenesis. ROC curve analysis indicated MD as the most predictive single parameter for Ki-67 expression (AUC = 0.762), showing significantly greater efficacy than D\* (Z = 2.022, P = 0.043). Thus, an MD value  $\leq 2.21 \times 10^{-3}$  mm²/s strongly suggests high tumor proliferative activity. In the training set, the combined models integrating select parameters from IVIM and DKI showed significantly higher predictive performance (AUCs: 0.852-0.923) compared to individual parameters. This

<sup>&</sup>lt;sup>2</sup>Department of Breast Surgery, Affiliated Hospital of Jining Medical University, Jining, China,

<sup>&</sup>lt;sup>3</sup>Department of Radiology, Yantai Yuhuangding Hospital, Qingdao University, Yantai, China,

<sup>&</sup>lt;sup>4</sup>Department of Cardiology, Affiliated Hospital of Jining Medical University, Jining, China, <sup>5</sup>Philips Healthcare, Beijing, China

performance was replicated in the external validation set (AUCs: 0.841-0.918), with no statistically significant difference in AUCs between the training and external validation sets according to DeLong's test (all P > 0.05). Moreover, the solid line provided a better approximation of the ideal dotted line, indicating higher predictive accuracy of the nomograms (P = 0.59, 0.40, and 0.08). According to the decision curve analysis (DCA), the predictive model provided a substantial net clinical benefit.

**Conclusion:** Our findings suggest that IVIM may be usefully combined with DKI to help predict the expression levels of Ki-67, HIF- $1\alpha$ , and VEGF in breast cancer, generating hypotheses for future research. Furthermore, the diagnostic efficiency of the parameters D\* and f appears to be enhanced by employing more low b-values (< $100-200 \text{ s/mm}^2$ ). These results require confirmation in prospective, multi-center studies.

KEYWORDS

diffusion-weighted imaging (DWI), diffusion kurtosis imaging (DKI), intravoxel incoherent motion (IVIM), hypoxia-inducible factor-1 alpha (HIF-1 $\alpha$ ), Ki-67, vascular endothelial growth factor (VEGF), apparent diffusion coefficient (ADC), true diffusion coefficient (D)

### Introduction

Breast carcinoma is currently recognized as a leading malignancy and primary contributor to cancer-related mortality in women. Moreover, recent trends indicate a growing incidence of breast cancer diagnoses among younger individuals (1). From a molecular viewpoint, breast carcinoma is a highly heterogeneous tumor type, posing considerable challenges for the accurate evaluation and implementation of personalized medicine into clinical practice (2). Factors such as tumor hypoxia, neovascularization, and proliferation contribute to the development of breast cancer heterogeneity, which has pivotal roles in the treatment response, prognosis, and recurrence of breast cancer (3, 4). Biomarkers including HIF-1α, Ki-67, and VEGF are recognized indicators of intratumoral heterogeneity, reflecting adaptive responses to hypoxia, proliferative activity, and angiogenic potential, respectively (5-7). Although biopsy remains the gold standard for diagnosis, its invasive nature and limited sampling constrain its ability to fully capture spatial and tumor heterogeneity. Thus, non-invasive imaging techniques capable of characterizing the tumor microenvironment comprehensively are increasingly needed.

In an era of personalized medicine, breast imaging becomes an essential component for breast cancer in terms of diagnosis, staging, treatment, and surveillance. Magnetic Resonance Imaging (MRI) is valuable in tumor disease assessment due to its freedom from ionizing radiation, high soft tissue resolution, multi-sequence imaging capability, and high repeatability properties (8). With the gradual refinement of tumor diagnosis and treatment, the

quantitative evaluation of tumor imaging has become increasingly important over the years (9). The DWI's ADC can reflect the water molecules' random movement (Brownian motion). However, the movement of water molecules within tissues may not be accurately represented by the ADC value due to the influence of blood microcirculation and tumor variability (10). Upon application of the double-exponential diffusion attenuation model, the IVIM can exhibit water molecules regarding tissue diffusion as well as perfusion parameters without using a contrast medium thus compensating for the limitations of traditional DWI (11). In addition, DKI can effectively account for the intricacy of tissue microstructure while providing diffusivity and kurtosis data, thereby yielding more accurate diffusion information (12). Therefore, multifunctional magnetic resonance imaging based on diffusion-weighted imaging provides a more accurate reflection of tumor heterogeneity.

Although DWI, IVIM, and DKI have been increasingly applied in predicting molecular markers across malignancies such as non-small cell lung cancer, hepatocellular carcinoma, endometrial carcinoma and breast carcinoma (13–17), few studies have systematically evaluated and compared the diagnostic performance of these techniques-both individually and in combination-for predicting HIF-1 $\alpha$ , Ki-67, and VEGF expression in breast cancer. Moreover, the potential of integrated models remain underexplored. Therefore, this study seeks to quantitatively assess and compare the value of DWI, IVIM, DKI, and combined models in predicting the expression levels of these biomarkers.

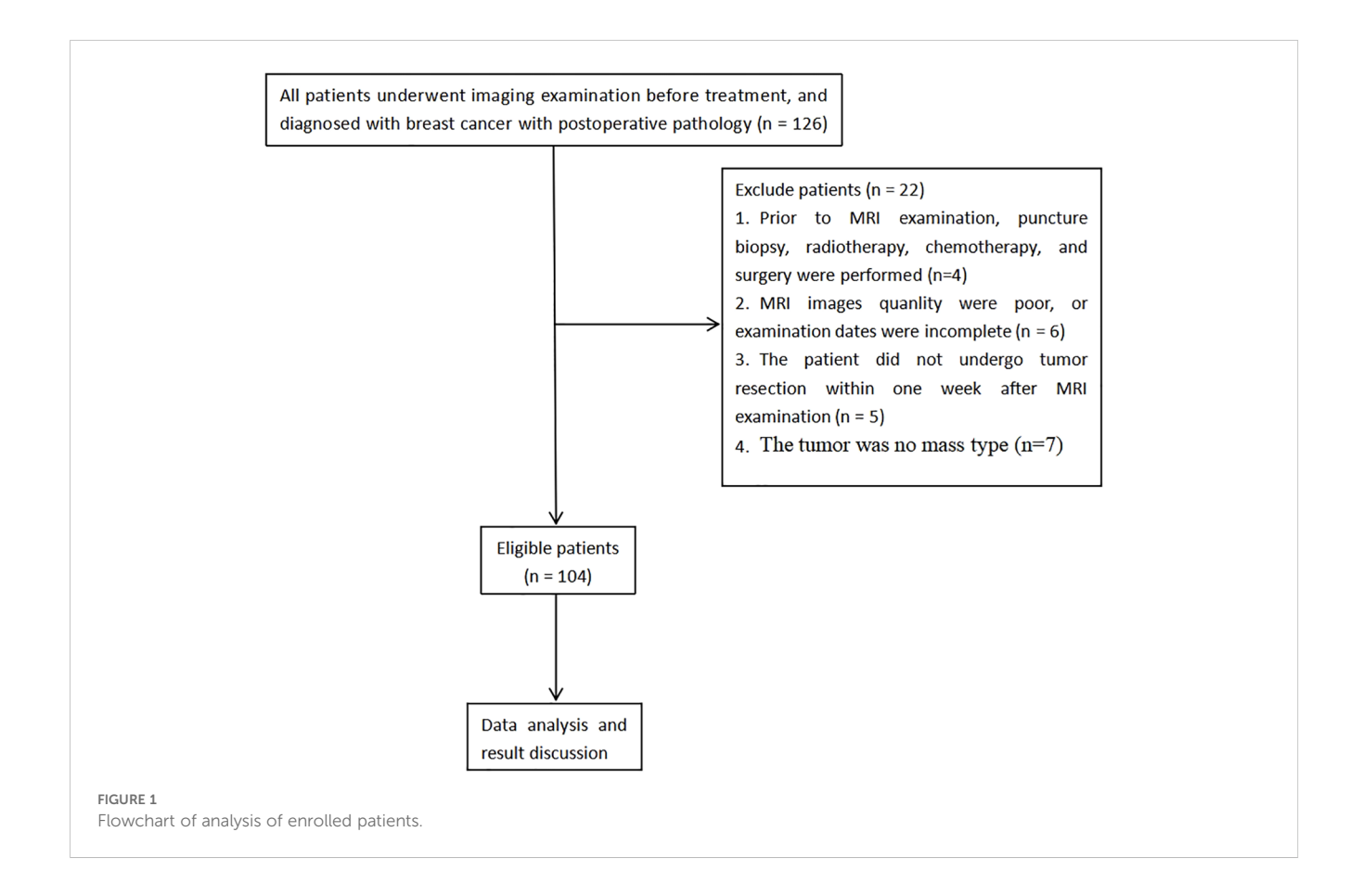
### Materials and methods

### Subjects and clinical factors

A total of 126 patients diagnosed with breast carcinoma, confirmed through pathological examination from January 2021 to December 2023, were recruited retrospectively. The adopted inclusion criteria involved: a) Subjects were all examined via conventional MRI, IVIM, and DKI, b) no contraindications for MRI examination, and c) complete clinicopathological data were obtained. The following exclusion criteria were implemented: a) patients who had undergone any prior treatment including core needle biopsy, radiotherapy, chemotherapy, or surgery before MRI examination, b) cases where MRI image quality was poor (defined as images with severe motion artifacts or insufficient signal-to-noise ratio for reliable ROI placement) or examination dates were incomplete, c) patients that had not undergone tumor resection within one week following MRI, and d) cases where the tumor did not present as a mass type. Ultimately, 104 patients who met the specified inclusion and exclusion parameters were enrolled for study (Figure 1). Additionally, 91 breast carcinoma patients were concurrently enrolled from another tertiary medical center, applying the same inclusion and exclusion criteria, to form an external validation cohort for assessing the model's generalizability.

### MRI technique

A GE Discovery 750W 3.0T MR scanner was utilized, featuring a dedicated 8-channel phased-array coil designed to encompass both breasts of all patients in a prone position. The MRI sequences included DKI, fast spin-echo T1-weighted imaging (FSE-T1WI), fat-suppressed fast-recovery fast spin-echo T2-weighted imaging (FRFSE-T2WI), DWI, and IVIM. The parameters employed to acquire FSE-T1WI images were as follows: echo time (TE)=10 ms, repetition time (TR) =420 ms, number of excitations (NEX)=1, and matrix =  $320 \times 288$ . The following sequences were employed to obtain FRFSE-T2WI images: TR = 6000 ms, TE = 88 ms, NEX = 2, matrix = 320×288. The DWI parameters were NEX = 2, TR = 3600 ms, matrix=320×288, TE = 73 ms, b-values=0, and 1000 s/mm<sup>2</sup>. The IVIM parameters were defined as follows: TE = 90 ms, thirteen b-values of 0, 20, 30, 50, 70, 100, 150, 200, 500, 700, 1000, 1500, 2000 s/mm<sup>2</sup>, matrix=128×128, NEX increased from 1 to 6, and TR = 2500 ms. DKI was acquired using the following sequence: NEX = 2, matrix=128×128, b-values at 0, 1000, 2000 s/mm<sup>2</sup>. TE = 90 ms, field of view (FOV)=35 cm $\times$ 35 mm, TR =



5000 ms, slice thickness=4 mm, and slice spacing= 0.4mm. The above sequence layers are all slice thickness=4mm, FOV = 35 cm×35 mm, and slice spacing=0.4mm.

### MRI evaluation

Processing of resulting data on DWI, IVIM, and DKI was completed by virtue of the Function tool MADC and DKI software (GE Healthcare, USA) to acquire parametric maps.

For DWI, ADC maps were generated using a mono-exponential model:  $S_b/S_0 = \exp(-b\cdot ADC)$ , where b denotes the diffusion factor, specifically, b=0 s/mm<sup>2</sup> for one volume and b=1000 s/mm<sup>2</sup> for the other (18).

The fitting equation reported previously was employed to calculate IVIM-derived parameters:  $S_b/S_0 = (1 - f) \times \exp(-b \times D) + f \times \exp[-b \times (D^* + D)]$ , where  $S_b$  represents the intensity of the MRI signal possessing diffusion weighting b,  $S_0$  the intensity of non-diffusion-weighted signal, and ADC the apparent diffusion coefficient. D signifies the true diffusion coefficient for water molecules concerning the pure diffusion. The pseudo-diffusion coefficient  $D^*$  corresponds to incoherent microcirculation related to perfusion and the microvascular volume fraction is denoted by the perfusion fraction f (18).

The parameters derived from DKI were obtained using the equation:  $S_b = S_0 \cdot \exp(-b^2 \cdot D^2 + b \cdot D^2 \cdot K/6)$ , where  $S_b$  and  $S_0$  correspond to signal intensities at different b-values (0 s/mm² and others, respectively). MD denotes the diffusion coefficient under normal conditions, adjusted for the non-Gaussian effects, while MK denotes non-Gaussian diffusion behavior (18).

Two radiologists (ZW with 5 years of experience together with WW having 8-year experience in breast MRI) who were blinded to all pathological results and clinical data, drew the ROIs independently. Since IVIM and DKI images displayed a low signal-to-noise ratio, the tumor's most enormous layers were selected to determine the ROI as per the DWI and T2WI images in the axial direction (b = 1000 s/ mm<sup>2</sup>). Three ROIs, each with 50~150 mm2 area, were drawn on the tumor's solid part, excluding the regions of cystic degeneration, bleeding, and necrosis as much as possible, and then copied the ROI onto the D, D \*, f, MD, and MK pseudocolor images. The average values of the quantitative parameters from both radiologists were calculated for final analysis. In cases of significant discrepancy in ROI placement (defined as a > 10% difference in measured value for any parameter), the images were jointly re-reviewed to reach a consensus. This approach, which focused on solid components, was chosen to minimize the confounding effects of necrosis and hemorrhage on parameter calculation, even though it may not fully capture the entire tumor's heterogeneity.

### Pathological assessments

All participating patients underwent surgical interventions, specifically, radical mastectomy, modified radical mastectomy, and breast-conserving surgery in 68, 24, and 12 cases, respectively. The

clinical database was utilized to extract multiple pathologic characteristics, such as histologic type, tumor size, ER/PR/HER-2/ HIF-1α/VEGF/Ki-67 status, histologic grade, tumor subtype, and patient age. All immunohistochemical evaluations of HIF-1 $\alpha$ , Ki-67, and VEGF were performed on postoperative surgical specimens obtained from the resected tumor mass. All surgically resected specimens were carried out by two independent pathologists (with working experience of 6 and 15 years), depending on levels of either estrogen receptor (ER), ki-67, human epidermal growth factor-2 (Her-2), as well as progesterone receptor (PR). Positivity for PR and ER was determined in cases where 10% or more nuclei exhibited positive staining. Ki-67 expression ≥14% was considered positive, while levels below this threshold were considered negative. Her-2 staining intensity was semiquantitatively scored 0 points for negative, 1+ point for weak, 2+ points for moderate or 3+ points for strong. The score of 0 or 1+ point meant Her-2 negative, while 3+ score was classified Her-2-positive. For tumors with a score of 2+ points, fluorescence in situ hybridization was conducted for further evaluation of gene amplification (19). Four distinct molecular subtypes of breast cancer were identified, namely, Her-2-positive (negative for ER and PR, Her-2-positive), luminal A (Her-2negative, positive for ER or PR, ki-67≥14%), triple-negative (negative for ER, PR and Her-2), and luminal B (negative for Her-2, positive for ER or PR, Ki-67<14%). Assessment of HIF-1α was conducted by calculating the ratio of cells with positive HIF-1 a to the total number of cells and scored as follows: 0 points (0-25%), 1 point (25-50%), 2 points (50-75%), 3 points (75-100%) and 4 points (100%). The intensity of staining was rated on a scale of 0 (no color), 1 (light yellow), 2 (brown), and 3 (dark brown) points. Low expression was defined by staining intensity <2 points alongside cells with positive HIF-1α <2 points. In contrast, a high expression was defined (20). The scoring system was applied to evaluate VEGF immunostaining based on the computed percentage of positive cells (0, no positive cells; 1,  $\leq$ 25% positive cells; 2, 25%< positive cells  $\leq$ 50%; 3, >50% positive cells) in addition to staining intensity (0=negative; 1=weak; 2=moderate; 3=high). The grading of these parameters yielded combined scores of 0-2, 3-4, and 5-6 corresponding to negative, positive, and strongly positive results, respectively (21).

### Statistical analysis

MedCalc 19.5.1 (Ostend, Belgium), R version 4.0.0 (http://www.r-project.org/), and SPSS 25.0 (IBM Corporation, Armonk, NY, USA) were employed for statistical analyses. The statistical analysis was performed under the supervision of a professional statistician (Juntao Zhang, GE Healthcare PDX GMS medical affairs, Senior Data Scientist). Interclass correlation coefficients (ICCs) were utilized to assess interobserver reproducibility. The criteria adopted for interpretation of ICC agreement were as follows: ICC  $\leq$  0.20, poor; 0.21<ICC  $\leq$  0.40, fair; 0.40<ICC  $\leq$  0.60, moderate; 0.60<ICC  $\leq$  0.80, good; 0.80<ICC  $\leq$  1.00, excellent (22). Two quantitative data samples were subjected to the Kolnogorov-Smirnov normality test to evaluate their distribution patterns. Data that followed normal and non-normal distribution were expressed as mean  $\pm$  standard deviation and median

plus interquartile range, respectively. The independent samples t-test was used for normally distributed data, and the Mann-Whitney U test was applied for non-normally distributed data. Different groups were compared using the independent-sample chi-square test. The binary logistic regression analysis was used to identify independent factors. Receiver operating characteristic (ROI) curves were performed to evaluate the diagnostic efficacy of each parameter or model. The Delong test analyzed the values of area under different groups' ROC curve (AUC). A nomogram was subsequently constructed and validated using decision curve analysis (DCA), together with calibration techniques. The Spearman rank was employed to describe the correlation of each parameter with HIF-1α, VEGF, and Ki-67, respectively. A correlation coefficient (r) of 0.75-1.00 was considered to indicate a good correlation, 0.50-0.74 a moderate correlation, 0.25-0.49 a mild correlation, and 0.24 or lower little or no correlation, p <0.05 denoted a difference of statistical significance (23).

### Results

### Clinical and pathological features

The 104 participants in the study had a mean age of  $52.99 \pm 9.58$  years, with an range from 29 to 71. Within this cohort of 104 cases of breast cancer, 95 (91.3%) were classified as invasive ductal carcinoma and 9 (8.7%) as non-invasive ductal carcinoma. Among the 104 patients, 11 (11%) were categorized as luminal A subtype, 19 (18%) as HER-2-positive subtype, 51 (49%) as luminal B subtype, and 23 (22%) as triple-negative subtype (Table 1). In the training set, no statistically significant differences were found in tumor genotypes between the high- and low-expression groups of HIF-1 $\alpha$ , VEGF, and Ki-67 (P = 0.42, 0.24, and 0.55, respectively). This lack of significant association was consistently observed in the external validation cohort, with corresponding P values of 0.22, 0.14, and 0.22.

### Interobserver agreement

The two radiologists reported ICCs of 0.887 [95% CI: 0.837–0.922], 0.917 [95% CI: 0.880–0.943], 0.860 [95% CI: 0.800–0.903], 0.880 [95% CI: 0.828–0.917], 0.909 [95% CI: 0.868–0.937], and 0.863 [95% CI: 0.805–0.905] for ADC, D, D\*, f, MD, and MK, respectively. These results reflect a significant level of agreement between observers.

### Diagnostic efficiency of DKI, DWI, and IVIM-derived parameters for HIF-1 $\alpha$ expression

In the training set, the D and MD values were significantly lower in tumors in the high-expression than the low-expression HIF-1 $\alpha$  group (p < 0.05). Additionally, the high-expression group was

TABLE 1 Clinical and pathological features of enrolled patients.

Feature	Date
Age (years), mean+SD	52.99 ± 9.58
Mean tumor size (cm), mean+SD	2.56 ± 1.09
Histologic grade, n (%)	
1	7 (6.7%)
2	44 (42.3%)
3	53 (51.0%)
Histologic type, n (%)	
Invasive ductal carcinoma	95 (91.3%)
Non-invasive ductal carcinoma	9 (8.7%)
ER, n (%)	
Negative (-)	42 (40%)
Positive (+)	62 (60%)
PR, n (%)	
Negative (-)	53 (51%)
Positive (+)	51 (49%)
HER-2, n (%)	
Negative (-)	51 (49%)
Positive (+)	53 (51%)
HIF-1α	
High	65 (62%)
Low	39 (38%)
VEGF	
High	64 (61%)
Low	40 (39%)
ki-67	
<14%	42 (40%)
>14%	62 (60%)
Tumor subtype, n (%)	
Luminal A	11 (11%)
Luminal B	51 (49%)
HER-2-positive	19 (18%)

HIF-10: Hypoxia inducible factor-alpha; ER: estrogen receptor; VEGF: vascular endothelial growth factor; PR: progesterone receptor.

observed with increased values of D\*, f, and MK compared with the low-expression group (p < 0.05). D [odds ratio(OR) = 0.001, P <0.001], D\* (OR = 1.805, P = 0.018), MD (OR = 0.168, P = 0.011), and MK (OR = 2034.665, P = 0.015) as significant predictive factors of HIF-1 $\alpha$ . ROC curve analysis showed that among the individual parameters, the D value exhibited the highest predictive efficacy (AUC = 0.724). A D value  $\leq 0.88 \times 10^{-3}$  mm²/s should strongly suggest high HIF-1 $\alpha$ 

expression. The AUC of the combined model incorporating MD, D, MK, and D\* was 0.860 with an accuracy of 77.9%, representing a modest but statistically significant improvement (Z=2.878~3.881, all P<0.05). A similar trend was observed in the external validation set. The combined model demonstrated comparable performance in the external validation set, achieving an AUC of 0.841, which was not significantly different from that in the training set (DeLong's test, Z = 0.262, P = 0.794). This indicates that the combined model provides a more reliable non-invasive assessment of tumor hypoxia (Tables 2, 3; Figures 2, 3).

### Diagnostic efficiency of DWI, IVIM, and DKI-derived parameters for VEGF expression

In the training set, comparative analyses revealed that relative to the low-expression group, the high-expression VEGF group had lower ADC, D, and MD values, along with higher D\*, MK, and f values (P<0.05). Furthermore, D (OR = 1.805, p = 0.018), f (OR = 1.805, p = 0.018), and MD (OR = 1.805, p = 0.018) served as independent predictors for assessing VEGF expression status. ROC curve analysis revealed that the f parameter was the most powerful single indicator for predicting VEGF expression (AUC = 0.882). The parameter f exhibited a significantly larger AUC than D and MD (Z = 2.036, P = 0.042; Z = 2.375, P = 0.018). In clinical practice, an f value ≥ 29.82% can serve as a key imaging biomarker suggesting high VEGF expression, i.e., active tumor angiogenesis. The combined model that incorporated D, f, and MD produced an AUC of 0.923, achieving an accuracy of 87.5%, demonstrating improved performance compared to the use of D or MD alone (Z = 3.357, P<0.001; Z = 3.927, P<0.001). Notably, however, the combined model did not significantly outperform f alone in terms of AUC (Z = 1.837, P = 0.066). A similar trend was observed in the external validation set. The generalizability of the combined model was further supported by the external validation results, which showed a consistently high AUC of 0.918. No statistically significant difference was found compared to the training set performance (DeLong's test,  $Z=0.089,\ P=0.929$ ). This suggests that the f parameter may play a central role in assessing angiogenesis (Tables 3, 4; Figures 2, 3).

### Diagnostic efficiency of DWI, IVIM, and DKI-derived parameters for Ki-67 expression

In the training set, the high-expression Ki-67 group exhibited significantly decreased ADC, D, and MD values, along with increased D\* and f values, compared to the low-expression group (P < 0.05). The parameters D (OR = 0.007, P = 0.002), D\* (OR = 1.080, p = 0.005), and MD (OR = 0.120, p = 0.002) emerged as predictors that could independently assess the status of Ki-67 expression. ROC curve analysis indicated MD as the most predictive single parameter for Ki-67 expression (AUC = 0.762), showing significantly greater efficacy than  $D^*$  (Z = 2.022, P = 0.043). Thus, an MD value  $\leq 2.21 \times 10^{-3}$  mm<sup>2</sup>/s strongly suggests high tumor proliferative activity. Furthermore, the combined model of D, D\*, and MD achieved an AUC of 0.852, with an accuracy of 77.9%, which was superior to that of the D, D\*, and MD parameters (Z=2.368~4.199, all P<0.05). A similar trend was observed in the external validation set. However, no statistically significant difference was found for the D\*parameter. No statistically significant difference was observed in the AUC values between the training set and the external validation set (AUC = 0.847) as assessed by DeLong's test (Z = 0.073, P = 0.942). This demonstrates the model's strong and generalizable predictive performance. This result indicates that integrating diffusion and perfusion information provides a more comprehensive perspective for the non-invasive assessment of tumor proliferation (Tables 3, 5; Figures 2, 3).

TABLE 2 Performance of the model combining IVIM and DKI in determination of the expression status of HIF-1α.

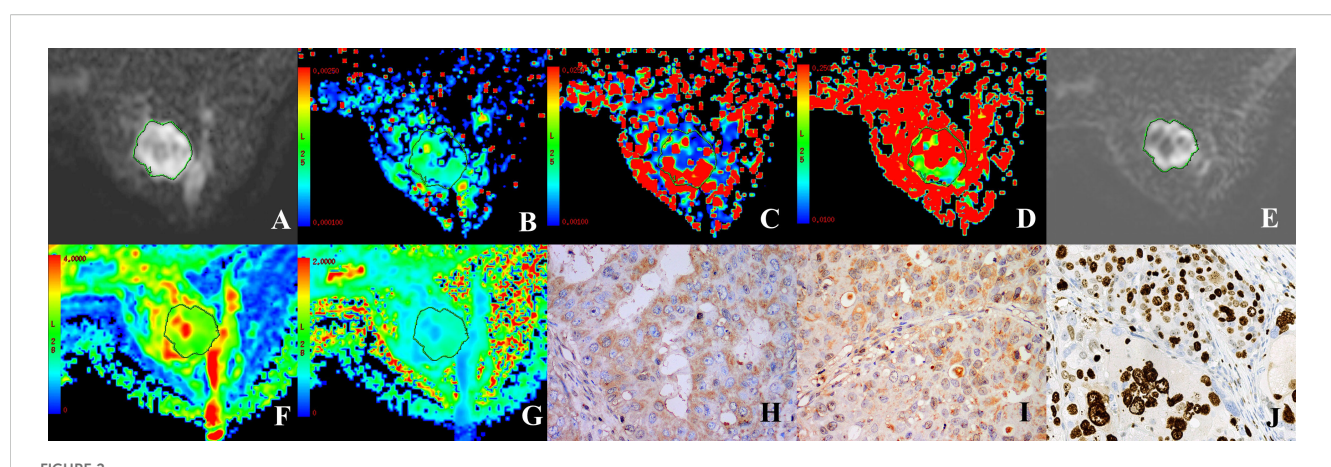
		Training (n = 104)	)	External validation (n = 91)			
Parameter	HIF	-1α	P-value	HIF	Divolue		
	High	Low	P-value	High	Low	P-value	
ADC (×10 <sup>-3</sup> mm <sup>2</sup> /s)	0.95 ± 0.09	0.97 ± 0.10	0.26	0.94 ± 0.09	0.96 ± 0.08	0.41	
D (×10 <sup>-3</sup> mm <sup>2</sup> /s)	0.82 ± 0.15	0.93 ± 0.16	0.001	0.81 ± 0.12	0.90 ± 013	0.001	
D* (×10 <sup>-3</sup> mm <sup>2</sup> /s)	26.29 (20.16, 47.28)	23.53 (18.52, 27.44)	0.003*	28.66 (15.23, 58.78)	26.42 (12.45, 41.35)	0.02*	
f (%)	31.73 (26.68, 36.36)	26.63 (21.73, 29.82)	0.007*	31.84 (16.37,45.15)	26.26 (18.54,46.89)	0.002*	
MD (×10 <sup>-3</sup> mm <sup>2</sup> /s)	2.16 ± 0.45	2.47 ± 0.52	0.002	2.08 ± 0.40	2.35 ± 0.50	0.005	
MK	0.78 ± 0.11	0.71 ± 0.14	0.006	0.75 ± 0.09	0.70 ± 0.13	0.03	

Date are presented as mean ± SD for normally distributed parameters (ADC, D, and MD) and median (IQR) for non-normally distributed parameters (D\*, f, and MK); HIF-1 $\alpha$ , Hypoxia inducible factor-alpha; MD, mean diffusion; ADC, apparent diffusion coefficient; MK, mean kurtosis; \*Mann-Whitney U test

TABLE 3 Performance of the model combining IVIM and DKI in determination of the expression status of HIF-1α, VEGF and ki-67.

Damanalana	Training (n = 104)				External validation (n = 91)							
Parameters	AUC	95%CI	Cutoff	Sensitivity (%)	Specificity (%)	Accuracy (%)	AUC	95%CI	Cutoff	Sensitivity (%)	Specificity (%)	Accuracy (%)
HIF-1α			1	1			,		1			
D	0.724	0.627-0.807	0.88	69.2	73.8	70.2	0.704	0.599-0.795	0.90	57.14	76.79	61.5
D*	0.674	0.575-0.763	32.73	94.9	47.7	59.6	0.652	0.545-0.749	37.55	97.14	33.93	64.8
MD	0.680	0.582-0.768	2.69	41.0	89.2	71.2	0.668	0.562-0.764	2.57	42.86	87.50	69.2
MK	0.665	0.565-0.754	0.68	56.4	84.6	70.2	0.644	0.537-0.742	0.68	48.57	80.36	68.1
Combined model	0.860	0.779-0.921	_	89.7	69.2	77.9	0.841	0.750-0.910	-	77.14	80.36	76.9
VEGF			•							:	•	
D	0.752	0.658-0.832	0.86	77.5	70.3	71.2	0.731	0.628-0.819	0.83	80.00	60.71	61.5
f	0.882	0.804-0.937	29.82	95.0	65.6	78.8	0.869	0.782-0.931	27.18	77.14	80.36	78.0
MD	0.744	0.649-0.824	2.03	80.0	56.3	66.3	0.701	0.596-0.793	1.98	74.29	62.50	67.0
Combined model	0.923	0.854-0.966	_	85.0	89.1	87.5	0.918	0.841-0.965	-	82.86	89.29	83.5
ki-67												
D	0.748	0.653-0.828	0.86	76.2	71.0	71.2	0.748	0.647-0.834	0.83	78.38	61.11	69.2
D*	0.607	0.506-0.701	35.71	90.5	40.3	54.8	0.611	0.503-0.712	37.55	94.59	33.33	60.4
MD	0.762	0.668-0.840	2.21	71.4	71.0	70.2	0.721	0.617-0.810	1.98	75.68	64.81	68.1
Combined model	0.852	0.769-0.914	-	85.7	72.6	77.9	0.847	0.757-0.914	-	81.08	75.93	75.8

Cut-off values were determined using Yonden's index; HIF-1 $\alpha$ , Hypoxia inducible factor-alpha; CI, confidence interval; MD, mean diffusion; MK, mean kurtosis; AUC, area under the ROC curve; VEGF, vascular endothelial growth factor.



A 37 year-old female patient with HER-2-positive cancer of the right breast. (**A, E**) Grayscale map (IVIM, DKI) presenting a b-value of 1000 s/mm<sup>2</sup> was selected to determine the ROI. (**B-D**) Maps in pseudo-colors for D, D\*, and (**F**) D =  $0.8 \times 10^{-3}$  mm<sup>2</sup>/s, D\*=71.49  $\times 10^{-3}$  mm<sup>2</sup>/s, f = 39.29%. (**F, G**) Maps in pseudo-colors for MD and MK. MD =  $1.85 \times 10^{-10^{-3}}$  mm<sup>2</sup>/s, MK = 0.84. (**H–J**) Immunohistochemical staining images for HIF-1 $\alpha$  (high expression), VEGF (strongly positive), and Ki-67 (positive) in cases of invasive ductal carcinoma of the breast.

## Predictive nomogram assessing the efficiency of parameters derived from DWI, IVIM, and DKI in determination of HIF- $1\alpha$ , VEGF, and Ki-67 expression

Based on the final regression analysis, we incorporated independent factors demonstrating significant associations with the diagnostic efficacy of parameters from DWI, IVIM, and DKI for expression of HIF-1α, VEGF, and Ki-67 into multivariate regression analysis, subsequently leading to the development of three nomograms (Figures 4A–C). Next, we evaluated the performance of the model by establishing internal calibration curves (Figures 4D–F). The probability of HIF-1α, VEGF, and ki-67 expression, as predicted via the nomogram, was set as the X-axis, with the actual probability represented on the Y-axis. The results showed that the ideal dotted line was more approximated by the solid line, suggesting

higher predictive accuracy of the nomograms (p = 0.59, 0.40, and 0.08). The decision curve analysis (DCA) described in Figures 4G–I highlights the excellent net clinical benefit of the predictive model.

### Correlation analysis

HIF-1 $\alpha$  showed mild positive correlations with D\*, f, and MK, respectively (r = 0.292, 0.267, 0.276, p<0.05). HIF-1 $\alpha$  was mildly correlated with D and MD, respectively (r = -0.375, -0.302, p<0.05). VEGF showed mild and moderate positive correlations with D\* and f, respectively (r = 0.390, 0.644, p<0.05). VEGF was mildly correlated with D and MD, respectively (r = -0.425, -0.411, p<0.05). Ki-67 showed mild positive correlations with D\* and f (r = 0.242, 0.308, p<0.05). Ki-67 was mildly correlated with D and MD, respectively (r = -0.422, -0.445, p<0.05).

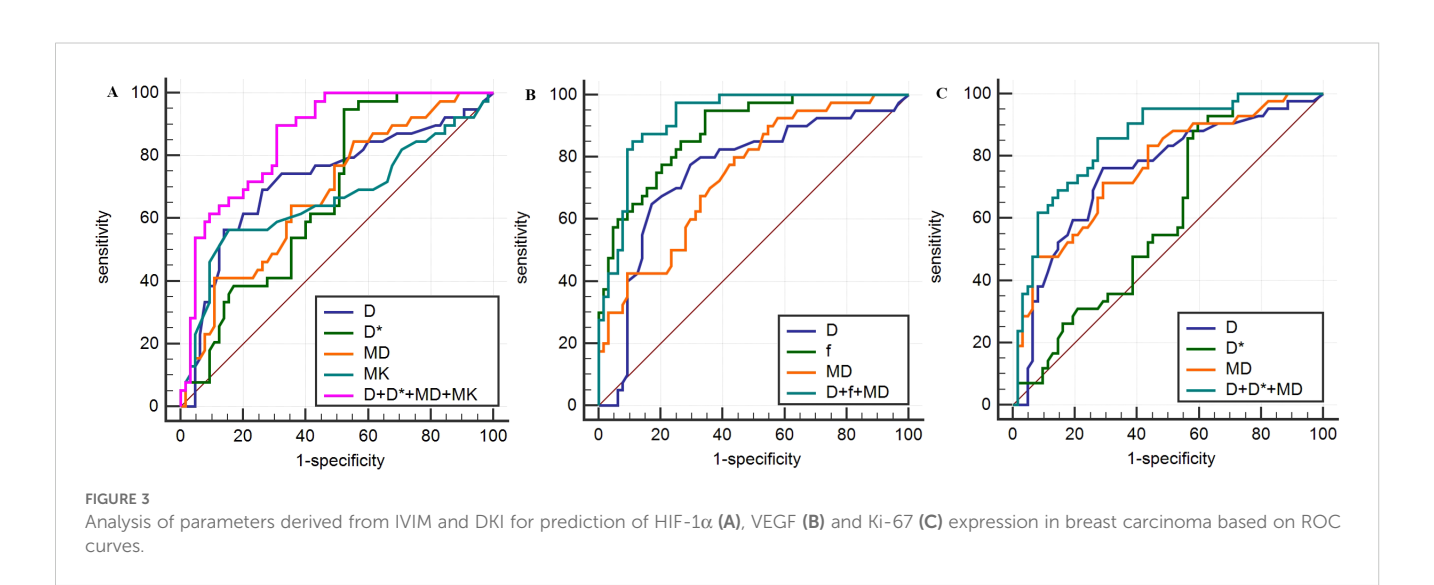


TABLE 4 Performance of the model combining IVIM and DKI in determination of the expression status of VEGF.

		Training (n = 104)	)	External validation (n = 91)			
Parameter	VE	GF	Dividica	VE	Danka		
	High	Low	P-value	High	Low	P-value	
ADC (×10 <sup>-3</sup> mm <sup>2</sup> /s)	0.94 ± 0.09	0.98 ± 0.09	0.019	0.92 ± 0.08	0.98 ± 0.08	0.002	
D (×10 <sup>-3</sup> mm <sup>2</sup> /s)	0.82 ± 0.16	0.94 ± 0.14	<0.001	0.81 ± 0.13	0.91 ± 0.12	<0.001	
D* (×10 <sup>-3</sup> mm <sup>2</sup> /s)	27.01 (21.41, 46.54)	20.30 (18.19, 27.43)	<0.001*	29.40 (15.23, 58.78)	25.03 (12.45, 36.98)	0.009*	
f (%)	32.30 (28.73, 38.15)	23.75 (19.78, 27.45)	<0.001*	32.52 (21.59,46.89)	23.59 (16.37,33.52)	<0.001*	
MD (×10 <sup>-3</sup> mm <sup>2</sup> /s)	2.11 ± 0.39	2.54 ± 0.54	<0.001	2.05 ± 0.39	2.39 ± 0.49	< 0.001	
MK	0.77 ± 0.12	0.72 ± 0.13	0.038	0.75 ± 0.10	0.71 ± 0.12	0.14	

Date are presented as mean ± SD for normally distributed parameters (ADC, D, and MD) and median (IQR) for non-normally distributed parameters (D\*, f, and MK); MD, mean diffusion; ADC, apparent diffusion coefficient; VEGF, vascular endothelial growth factor; MK, mean kurtosis; \*Mann-Whitney U test

### Discussion

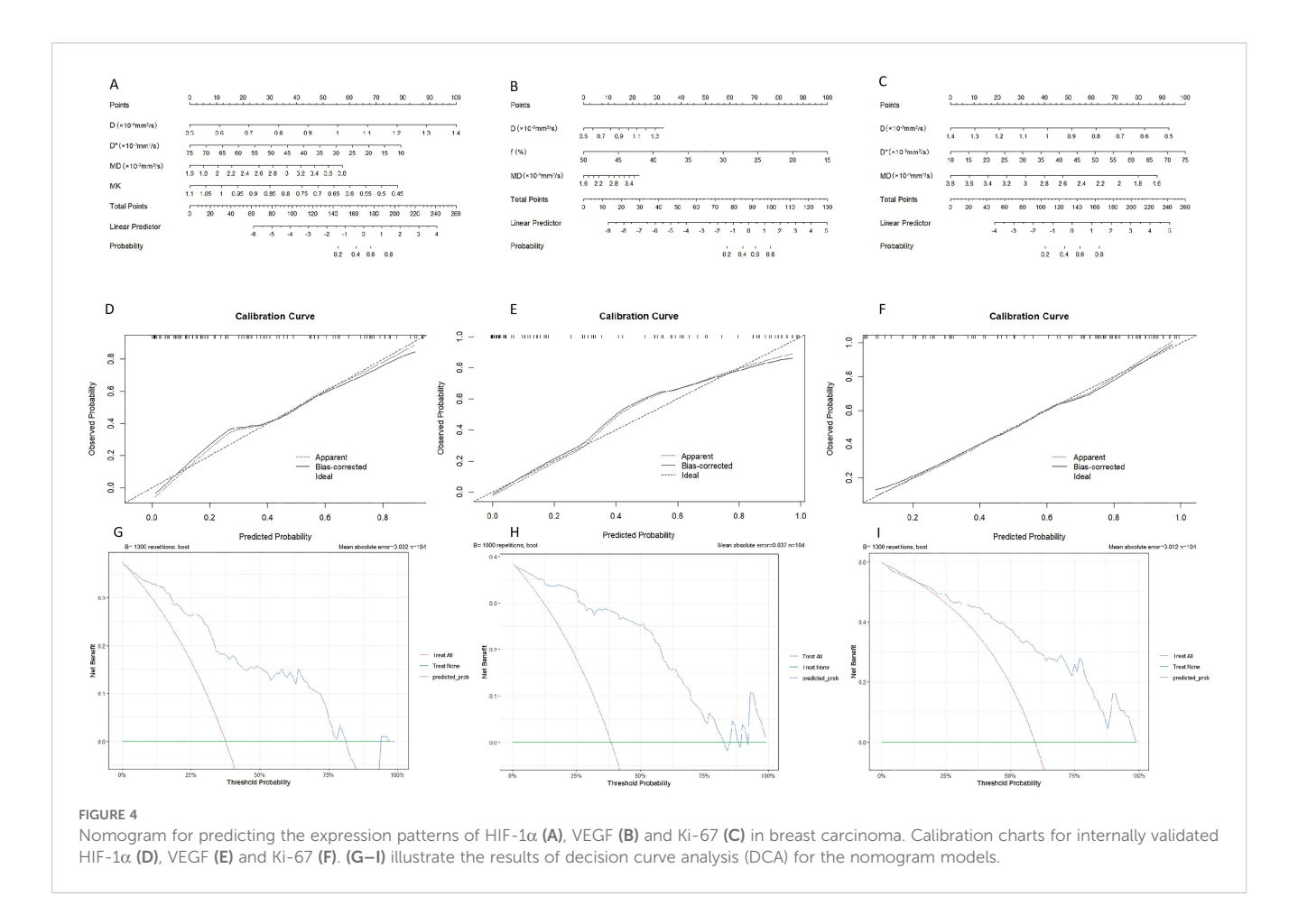
Breast cancer is a multifaceted disease featuring uncontrolled cell growth. The rapid propagation of breast tumor cells is reflected by elevated Ki-67 expression (24). This study demonstrated decreased ADC, D, and MD values in the groups showing high Ki-67 expression relative to those with low expression, in keeping with findings documented in numerous earlier studies (17, 25, 26). The biological mechanism underlying this phenomenon is rooted in the fact that highly proliferative tumor cells result in a substantial increase in cellular density. This increase significantly restricts the diffusion of water molecules, leading to a deviation from Gaussian distribution. According to Meng et al. (17), efficient prediction of high and low Ki-67 expression using the ADC value poses a considerable challenge. This discrepancy may be ascribed to ADC demonstrating the proper diffusion of water molecules together with "false diffusion" caused by the blood microcirculation within capillaries. In this study, the high ki-67 expression group when contrasted with the low expression group exhibited higher values of D\* and f, suggesting that the tumor tissue maintains high perfusion levels. However, other investigations have reported no significant correlation between D\* and f values and Ki-67 expression (25, 27). Our in-depth analysis suggests that these discrepancies could be closely related to the selection strategy of b-values below 100-200 s/ mm<sup>2</sup> in IVIM sequences, as these low b-values were sensitive to perfusion effects. Research by Zhang et al. (25) demonstrated that a few b-values less than 100-200 s/mm<sup>2</sup> could reduce the predictive efficiency of parameters D\* and f. In this study, the IVIM sequence was selected to set 13 b values, among which 8 were lower than 200 s/mm<sup>2</sup>. The parameters D, D\*, and MD were identified as independent predictors of the Ki-67 expression status. Our results further showed that MD had the highest AUC compared with D and D\* parameters, which could be attributed to the enhanced ability of DKI to precisely measure the diffusion of water molecules. Additionally, ROC analysis demonstrated that the model combining all three quantitative parameters outperformed the individual parameters. The model demonstrated robust performance in the training cohort and, more importantly, this strong predictive ability was successfully replicated in the external validation set. This finding suggests that an integrated multi-model approach holds promise for enhancing the non-invasive prediction accuracy of Ki-67 expression status in breast cancer. Consequently, it offers a more comprehensive imaging basis for the preoperative assessment of tumor proliferative activity.

Solid tumors commonly exhibit hypoxia, which arises from the rapid proliferation and intense metabolic activity of tumor cells.

TABLE 5 Performance of the model combining IVIM and DKI in determination of the expression status of Ki-67.

	-	Training (n = 104)	)	External validation (n = 91)			
Parameter	Ki-	-67	Duralina	Ki-	Danka		
	High	Low	P-value	High	Low	P-value	
ADC (×10 <sup>-3</sup> mm <sup>2</sup> /s)	0.94 ± 0.10	0.98 ± 0.10	0.047	0.93 ± 0.09	0.97 ± 0.09	0.036	
D (×10 <sup>-3</sup> mm <sup>2</sup> /s)	0.82 ± 0.16	0.94 ± 0.14	<0.001	0.80 ± 0.12	0.91 ± 0.13	<0.001	
D* (×10 <sup>-3</sup> mm <sup>2</sup> /s)	33.71 ± 16.41	25.69 ± 8.20	0.004	27.83 (15.23,58.78)	25.46 (12.45,45.89)	0.072*	
f (%)	31.78 (26.93, 36.82)	26.60 (21.73, 29.77)	0.002*	31.65 (16.37,45.15)	26.45 (18.54,46.89)	0.004*	
MD (×10 <sup>-3</sup> mm <sup>2</sup> /s)	2.10 ± 0.40	2.54 ± 0.51	<0.001	2.03 ± 0.37	2.40 ± 0.49	<0.001	
MK	0.77 ± 0.11	0.73 ± 0.14	0.072	0.74 ± 0.09	0.71 ± 0.13	0.109	

Date are presented as mean  $\pm$  SD for normally distributed parameters (ADC, D, and MD) and median (IQR) for non-normally distributed parameters (D\*, f, and MK); MD, mean diffusion; ADC, apparent diffusion coefficient; MK, mean kurtosis; \*Mann-Whitney U test



HIF-1α has been established as the most important regulatory element in the hypoxic responses of tumor cells (5). Here, we observed that compared to the low HIF-1 $\alpha$  expression group, the high expression group exhibited lower values of D and MD, along with higher D\*, f, and MK values, consistent with previous results (28, 29). We propose the following mechanistic explanations for these findings: (1) HIF-1α promotes glucose uptake by tumor cells, enhancing their proliferation and metabolic ability, leading to enhanced cellular density that restricts water molecule diffusion (30); (2) HIF-1 $\alpha$  is known to stimulate tumor angiogenesis by regulating downstream factors such as VEGF, consequently increasing tissue perfusion (31). Notably, the study by Li et al. (28) reported no significant correlation between HIF-1α expression and D\*. This discrepancy again underscores the substantial impact of technical protocols in IVIM imaging, particularly the setting of low b-values, on the comparability of research findings. The above study only selected six b values set below 200 s/mm<sup>2</sup>. Data from the present investigation indicate that D, D\*, MD and MK acted as factors capable of independently assessing the status of HIF-1α expression. The D (70.2%) had the highest predictive power. Both MD (71.2%) and MK (70.2%) showed superior accuracy, possibly due to the ability of DKI to not only efficiently quantify water molecules for non-Gaussian diffusion features in tissues but also provide more accurate and reliable information regarding tissue microstructure (12). Moreover, the combination of D, D\*, MD and MK exhibited greater predictive accuracy compared to each individual parameter. Furthermore, the successful external validation indicates that our model could serve as a reliable tool for non-invasive assessment of tumor hypoxia across different institutions, thereby supporting clinical decision-making. Therefore, utilizing such a combined model can enhance the prediction of HIF- $1\alpha$ , which holds potential implications for estimating tumor sensitivity to radiotherapy or targeted therapies, as hypoxia is often associated with treatment resistance.

VEGF, which facilitates the angiogenic process, serves as a quantitative index for evaluating angiogenesis in tumors (6). In contrast to the VEGF low-expression group, the high-expression group presented elevation of D\* and f values, in alignment with previous research findings (15, 32). This variation could be explained by the stimulatory influence of VEGF expression on angiogenesis, thereby enhancing tumor perfusion. Furthermore, relative to the low-expression group, the high-expression group showed lower ADC and D values. This observation may be attributed to the ability of VEGF to induce angiogenesis, thereby supplying the increased nutrient requirement for proliferation, increasing cell density, and further limiting the diffusion of water molecules. In contrast, Yang et al. (15) found that patients with varying VEGF expression levels showed no significant differences in ADC and D values. The reason for this difference may be that VEGF expression results in a higher speed of proton movement in lumens

together with a larger number of tumor blood vessels (33). Our study indicated that compared with the VEGF low-expression group, the high-expression group showed a decline in MD values and concomitant increase in MK values, consistent with previous findings (34), possibly because VEGF accelerates cell proliferation and tumor growth, resulting in high tumor heterogeneity and significant deviation of water diffusion from the Gaussian distribution. The values of D, f and MD served as independent variables for assessing the VEGF expression status. Notably, AUC for f was significantly greater than those of the other parameters. Additional ROC analysis indicated that the composite model utilizing the three quantitative parameters provided superior diagnostic performance compared to the individual parameters. Nonetheless, no substantial differences were observed between the f value and the composite model, clearly implying that f serves as the most promising parameter for distinguishing VEGF expression. This has direct clinical relevance, as anti-angiogenic therapies target the VEGF pathway. The IVIM-derived f parameter provides a noninvasive method for assessing tumor perfusion. In the future, it could be used to screen patients for potential benefit from antiangiogenic therapy or to monitor early treatment response.

Our research has a number of specific limitations that warrant careful consideration. Firstly, the study was conducted on a limited patient cohort, which could potentially introduce bias into the findings. Secondly, the solid components of the tumor were primarily determined as the ROI, rather than encompassing the entire breast cancer, which may not adequately capture the full extent of tumor heterogeneity. Thirdly, we have not yet achieved precise location of MRI and pathology "face to face". Fourthly, our ROI analysis was restricted to the solid portion of the tumors, and non-mass lesions were excluded. This may introduce selection bias and limit the generalizability of our findings. Fifthly, the precise optimal number of b-values below 100-200 s/mm<sup>2</sup> for IVIM imaging in breast cancer remains to be determined. Future studies should focus on larger sample sizes, incorporate wholetumor ROIs to address heterogeneity, improve MRI-pathology alignment, and optimize low b-values for IVIM imaging to enhance the accuracy and clinical applicability of breast cancer characterization. Finally, the external cohort was recruited from a single center with a limited sample size. Future multi-center studies with larger, prospective cohorts are essential to further confirm these findings and facilitate clinical translation.

In summary, the findings from this retrospective study suggest the potential of a multiparametric MRI approach combining IVIM and DKI for non-invasive assessment of tumor biology in breast cancer. Overall, MD appears to serve as a more reliable predictor of Ki-67 expression relative to parameters derived from IVIM, while the f parameter is the most beneficial for distinguishing VEGF expression compared to other functional indicators from IVIM and DKI. The efficacy in assessing HIF-1α expression is enhanced by the D parameter from IVIM, alongside MD and MK from DKI. These hypothesis-generating results highlight a promising direction for future research. In the training set, combined models integrating select parameters from IVIM and DKI showed significantly higher predictive performance (AUCs: 0.852-0.923) compared to

individual parameters. While the gain in AUC may be modest, the model's value lies in its synthesis of complementary biological information-water diffusion, microcirculatory perfusion, and structural complexity-into a more holistic assessment. In addition, the successful external validation of our model demonstrates not only its exceptional generalizability but also its robustness against overfitting. By applying a wider range of b values, specifically those below 100–200 s/mm², the stability and accuracy of D\* and f measurements could be significantly improved. Furthermore, our results suggest that utilizing large quantities of b-values below 100–200 s/mm² could enhance the diagnostic efficiency of D\* and f parameters.

### Data availability statement

The original contributions presented in the study are included in the article/supplementary material. Further inquiries can be directed to the corresponding authors.

### **Ethics statement**

The studies involving humans were approved by the Institutional Review Board of the Affiliated Hospital of Jining Medical University. The studies were conducted in accordance with the local legislation and institutional requirements. The participants provided their written informed consent to participate in this study. Written informed consent was obtained from the individual(s) for the publication of any potentially identifiable images or data included in this article.

### **Author contributions**

ZW: Conceptualization, Writing - original draft, Investigation, Writing - review & editing, Methodology, Project administration, Formal Analysis, Data curation. FZ: Formal Analysis, Project administration, Writing - original draft, Methodology, Conceptualization, Investigation, Data curation. LZ: Methodology, Project administration, Investigation, Formal Analysis, Data curation, Writing - original draft, Conceptualization. NM: Writing - orginal draft, Data curation, Resources. WW: Conceptualization, Data curation, Resources, Validation, Writing - review & editing, Project administration, Writing original draft, Methodology. WZ: Data curation, Writing original draft, Formal Analysis, Funding acquisition, Software. HY: Formal Analysis, Software, Data curation, Writing - original draft. YL: Software, Data curation, Writing - original draft, Formal Analysis. CL: Writing - original draft, Resources, Data curation. XY: Methodology, Formal Analysis, Data curation, Software, Writing - original draft. YC: Visualization, Validation, Conceptualization, Writing - original draft, Supervision, Project administration. ZS: Writing - original draft, Funding acquisition, Resources, Visualization, Project administration, Data curation,

Validation, Conceptualization, Writing – review & editing, Supervision, Methodology.

### **Funding**

The author(s) declare financial support was received for the research and/or publication of this article. This work was supported by the Research Fund for Academician Lin He New Medicine (Grant number: JYHL2022FMS07) and the Key R&D Program of Jining (Grant number: 2023YXNS133).

### Conflict of interest

Author XY was employed by company Philips Healthcare.

The remaining authors declare that the research was conducted in the absence of any commercial or financial relationships that could be construed as a potential conflict of interest.

### References

- 1. Zhou J, Wu L, Xu P, Li Y, Ji Z, Kang X. Filamin A is a potential driver of breast cancer metastasis via regulation of MMP-1. *Front Oncol.* (2022) 12:836126. doi: 10.3389/fonc.2022.836126
- 2. Li X, Xia S, Zhou W, Ji R, Zhan W. Targeted Fe-doped silica nanoparticles as a novel ultrasound-magnetic resonance dual-mode imaging contrast agent for HER2-positive breast cancer. *Int J Nanomedicine*. (2019) 14:2397–413. doi: 10.2147/IJN.S189252
- 3. Tang K, Zhu L, Chen J, Wang D, Zeng L, Chen C, et al. Hypoxia promotes breast cancer cell growth by activating a glycogen metabolic program. *Cancer Res.* (2021) 81:4949–63. doi: 10.1158/0008-5472.CAN-21-0753
- 4. Lin L, Tong X, Hu P, Invernizzi M, Lai L, Wang LV. Photoacoustic computed tomography of breast cancer in response to neoadjuvant chemotherapy. *Adv Sci (Weinh)*. (2021) 8:2003396. doi: 10.1002/advs.202003396
- 5. Cowman SJ, Koh MY. Revisiting the HIF switch in the tumor and its immune microenvironment. *Trends Cancer.* (2022) 8:28–42. doi: 10.1016/j.trecan.2021.10.004
- 6. Ghalehbandi S, Yuzugulen J, Pranjol MZI, Pourgholami MH. The role of VEGF in cancer-induced angiogenesis and research progress of drugs targeting VEGF. Eur J Pharmacol. (2023) 949:175586. doi: 10.1016/j.ejphar.2023.175586
- 7. Memon SS, Guruvayoorappan C, Sakthivel KM, Rasmi RR. Ki-67 protein as a tumor proliferation marker. *Clin Chim Acta*. (2019) 491:39–45. doi: 10.1016/j.cca.2019.01.011
- 8. Wekking D, Porcu M, Silva PD, Saba L, Scartozzi M, Solinas C. Breast MRI: clinical indications, recommendations, and future applications in breast cancer diagnosis. *Curr Oncol Rep.* (2023) 25:257–67. doi: 10.1007/s11912-023-01372-x
- 9. Jiang X, Jia H, Zhang Z, Wei C, Wang C, Dong J. The feasibility of combining ADC value with texture analysis of  $T_2WI$ , DWI and CE- $T_1WI$  to preoperatively predict the expression levels of Ki-67 and p53 of endometrial carcinoma. *Front Oncol.* (2021) 11:805545. doi: 10.3389/fonc.2021.805545
- 10. Rahmat K, Mumin NA, Hamid MTR, Hamid SA, Ng WL. MRI breast: current imaging trends, clinical applications, and future research directions. *Curr Med Imaging*. (2022) 18:1347–61. doi: 10.2174/1573405618666220415130131
- 11. Iima M. Perfusion-driven intravoxel incoherent motion (IVIM) MRI in oncology: applications, challenges, and future trends. *Magn Reson Med Sci.* (2021) 20:125–38. doi: 10.2463/mrms.rev.2019-0124
- 12. Zhang D, Geng X, Suo S, Zhuang Z, Gu Y, Hua J. The predictive value of DKI in breast cancer: Does tumour subtype affect pathological response evaluations? *Magn Reson Imaging*. (2022) 85:28–34. doi: 10.1016/j.mri.2021.10.013
- 13. Surov A, Clauser P, Chang YW, Li L, Martincich L, Partridge SC, et al. Can diffusion-weighted imaging predict tumor grade and expression of Ki-67 in breast cancer? A multicenter analysis. *Breast Cancer Res.* (2018) 20:58. doi: 10.1186/s13058-018-0991-1
- 14. Huang Z, Xu X, Meng X, Hou Z, Liu F, Hua Q, et al. Correlations between ADC values and molecular markers of Ki-67 and HIF-1 $\alpha$  in hepatocellular carcinoma. *Eur J Radiol.* (2015) 84:2464–9. doi: 10.1016/j.ejrad.2015.09.013

### Generative AI statement

The author(s) declare that no Generative AI was used in the creation of this manuscript.

Any alternative text (alt text) provided alongside figures in this article has been generated by Frontiers with the support of artificial intelligence and reasonable efforts have been made to ensure accuracy, including review by the authors wherever possible. If you identify any issues, please contact us.

### Publisher's note

All claims expressed in this article are solely those of the authors and do not necessarily represent those of their affiliated organizations, or those of the publisher, the editors and the reviewers. Any product that may be evaluated in this article, or claim that may be made by its manufacturer, is not guaranteed or endorsed by the publisher.

- 15. Yang C, Wei XQ, Zheng J, Tao YY, Gong XQ, Li L, et al. A correlative study between IVIM-DWI parameters and VEGF and MMPs expression in hepatocellular carcinoma. *Quant Imaging Med Surg.* (2023) 13:1887–98. doi: 10.21037/qims-22-271
- 16. Zheng Y, Huang W, Zhang X, Lu C, Fu C, Li S, et al. A Noninvasive Assessment of Tumor Proliferation in Lung cancer Patients using Intravoxel Incoherent Motion Magnetic Resonance Imaging. *J Cancer.* (2021) 12:190–7. doi: 10.7150/jca.48589
- 17. Meng H, Ding SX, Zhang Y, Zhu FY, Wang J, Wang JN, et al. Value of multimodal diffusion-weighted imaging in preoperative evaluation of Ki-67 expression in endometrial carcinoma. *Curr Med Imaging*. (2023). doi: 10.2174/1573405620666230811142710
- 18. Wang W, Zhang X, Zhu L, Chen Y, Dou W, Zhao F, et al. Prediction of prognostic factors and genotypes in patients with breast cancer using multiple mathematical models of MR diffusion imaging. *Front Oncol.* (2022) 12:825264. doi: 10.3389/fonc.2022.825264
- 19. Zhao M, Fu K, Zhang L, Guo W, Wu Q, Xue B, et al. Intravoxel incoherent motion magnetic resonance imaging for breast cancer: A comparison with benign lesions and evaluation of heterogeneity in different tumor regions with prognostic factors and molecular classification. *Oncol Lett.* (2018) 16:5100–12. doi: 10.3892/ol.2018.9312
- 20. Li X, Wu S, Li D, Yu T, Zhu H, Song Y, et al. Intravoxel incoherent motion combined with dynamic contrast-enhanced perfusion MRI of early cervical carcinoma: correlations between multimodal parameters and HIF-1 $\alpha$  Expression. *J Magn Reson Imaging.* (2019) 50:918–29. doi: 10.1002/jmri.26604
- 21. Li Y, Wei X, Zhang S, Zhang J. Prognosis of invasive breast cancer after adjuvant therapy evaluated with VEGF microvessel density and microvascular imaging.  $Tumour\ Biol.\ (2015)\ 36:8755-60.\ doi: 10.1007/s13277-015-3610-0$
- 22. Tu C, Shen H, Liu R, Wang X, Li X, Yuan X, et al. Myocardial extracellular volume derived from contrast-enhanced chest computed tomography for longitudinal evaluation of cardiotoxicity in patients with breast cancer treated with anthracyclines. *Insights Imaging.* (2022) 13:85. doi: 10.1186/s13244-022-01224-5
- 23. Kun S, Chen X, Chai W, Fei X, Fu C, Yan X, et al. Breast cancer: diffusion kurtosis MR imaging-diagnostic accuracy and correlation with clinical-pathologic factors. *Radiology*. (2015) 277:46–55. doi: 10.1148/radiol.15141625
- 24. Yu H, Meng X, Chen H, Han X, Fan J, Gao W, et al. Correlation between mammographic radiomics features and the level of tumor-infiltrating lymphocytes in patients with triple-negative breast cancer. *Front Oncol.* (2020) 10:412. doi: 10.3389/fonc.2020.00412
- 25. Zhang K, Dai Y, Liu Y, Tao J, Pan Z, Xie L, et al. Soft tissue sarcoma: IVIM and DKI parameters correlate with Ki-67 labeling index on direct comparison of MRI and histopathological slices. *Eur Radiol.* (2022) 32:5659–68. doi: 10.1007/s00330-022-08646-1
- 26. Wang F, Wu L, Hua XL, Zhao ZZ, Chen XX, Xu JR. Intravoxel incoherent motion diffusion-weighted imaging in assessing bladder cancer invasiveness and cell proliferation. *J Magn Reson Imaging*. (2018) 47:1054–60. doi: 10.1002/jmri.25839

- 27. Song XL, Wang L, Ren H, Wei R, Ren JL, Niu J. Intravoxel incoherent motion imaging in differentiation borderline from Malignant ovarian epithelial tumors: correlation with histological cell proliferation and vessel characteristics. *J Magn Reson Imaging*. (2020) 51:928–35. doi: 10.1002/jmri.26885
- 28. Li X, Yang L, Wang Q, Tao J, Pan Z, Wang S. Soft tissue sarcomas: IVIM and DKI correlate with the expression of HIF-1 $\alpha$  on direct comparison of MRI and pathological slices. Eur Radiol. (2021) 31:4669–79. doi: 10.1007/s00330-020-07526
- 29. Duan Z, Tao J, Liu W, Liu Y, Fang S, Yang Y, et al. Correlation of IVIM/DKI parameters with hypoxia biomarkers in fibrosarcoma murine models: direct control of MRI and pathological sections. *Acad Radiol.* (2024) 31:1014–23. doi: 10.1016/j.acra.2023.08.021
- 30. Lee JH, Yoon YC, Seo SW, Choi YL, Kim HS. Soft tissue sarcoma: DWI and DCE-MRI parameters correlate with Ki-67 labeling index. *Eur Radiol.* (2020) 30:914–24. doi: 10.1016/j.acra.2023.08.021
- 31. Patra K, Jana S, Sarkar A, Mandal DP, Bhattachrjee S. The inhibition of hypoxia-induced angiogenesis and metastasis by cinnamaldehyde is mediated by decreasing HIF-1 $\alpha$  protein synthesis via PI3K/Akt pathway. *Biofactors*. (2019) 45:401–15. doi: 10.1002/biof.1499
- 32. Gao P, Liu Y, Shi C, Liu Y, Luo L. Performing IVIM-DWI using the multifunctional nanosystem to evaluate the antitumor microcirculation changes. MAGMA. (2020) 33:517–26. doi: 10.1007/s10334-019-00814-7
- 33. Li JL, Ye WT, Liu ZY, Yan LF, Luo W, Cao XM, et al. Comparison of microvascular perfusion evaluation among IVIM-DWI, CT perfusion imaging and histological microvessel density in rabbit liver VX2 tumors. *Magn Reson Imaging*. (2018) 46:64–9. doi: 10.1016/j.mri.2017.10.014
- 34. Shi RY, Yao QY, Zhou QY, Lu Q, Suo ST, Chen J, et al. Preliminary study of diffusion kurtosis imaging in thyroid nodules and its histopathologic correlation. *Eur Radiol.* (2017) 27:4710–20. doi: 10.1007/s00330-017-4874-0